ORIGINAL PAPER

Enhancing brilliant green dye adsorption-photodegradation using a TiO$_2$-modified natural material

Mohamed Belghiti[1,3] · Karim Tanji[2,7] · Youssef Fahoul[2] · Lekbira El Mersly[3] · Redouane Haounati[4] · Imane El Mrabet[5] · El Mountassir El Mouchtari[3] · Salah Rafqah[3] · Abdelhak Kherbeche[2] · Hicham Zaitan[6]

Abstract

The present study investigates the photocatalytic degradation of Brilliant Green (BG) dye using a modified natural material (NM) incorporated with titanium dioxide (TiO$_2$) under ultraviolet (UV) irradiation. The synthesized catalyst NM-TiO$_2$-20% was evaluated for degrading BG dye. An optimization process was carried out using a Box-Behnken design to maximize the removal efficiency of BG dye. The optimal parameters obtained were %TiO$_2$ = 20%, [BG] = 38.02 ppm, and pH = 9.91, resulting in a remarkable removal efficiency of 98.82%. Moreover, NM-TiO$_2$-20% exhibited remarkable stability over five cycles. Additionally, the scavenging tests of free radicals indicate the involvement of superoxide ions (O$_2^{\bullet-}$) and hydroxyl radicals ($^{\bullet}$OH) as the species responsible for BG degradation. The present findings underscore the synergistic effect between the low-cost natural material and pristine TiO$_2$ (this means the synergy effect of adsorption and photocatalysis combination) on the photodegradation of BG dye, as an organic pollutant in contaminated wastewater. This confirms the potential of utilizing natural materials for promising and sustainable depollution applications with NM-based photocatalysts. In this study, NM-TiO$_2$-20% was identified as the optimal and most effective system, achieving almost complete elimination of the dye molecules compared to NM alone, TiO$_2$ alone, NM-TiO$_2$-10%, and NM-TiO$_2$-15%.

Keywords Photocatalytic degradation · UV light · Brilliant Green · Wet impregnation · Box-Behnken optimization

Introduction

The contamination of water bodies by synthetic dyes, particularly those used in various industrial processes, presents a significant environmental challenge. These dyes are often

Responsible Editor: Mongi Seffen.

✉ Karim Tanji
karim.tanji@usmba.ac.ma

1   Laboratory of Nanomaterials, Energy and Environment, Faculty of Sciences Semlalia, Cadi Ayyad University, BP 2390, 40000 Marrakech, Morocco

2   Laboratory of Materials, Processes, Catalysis and Environment (LMPCE), Higher School of Technology of Fez, Sidi Mohamed Ben Abdallah University, Fez, Morocco

3   Laboratory of Analytical and Molecular Chemistry, Polydisciplinary Faculty of Safi, Cadi Ayyad University, Safi, Morocco

4   Chemical and Biochemical Sciences, Green Process Engineering, Mohammed, VI Polytechnic University (UM6P), Lot 660—Hay Moulay Rachid, 43150 Ben Guerir, Morocco

5   Team of Applied Chemistry, Geo-Mining and Modeling (CAG2M), Polydisciplinary Faculty of Ouarzazate, Ibnou Zohr University, Ouarzazate, Morocco

6   Processes, Materials and Environment Laboratory (LPME), Faculty of Sciences and Technology of Fez, Sidi Mohamed Ben Abdallah University, BP 2202, Fez, Morocco

7   Laboratory of Advanced Materials and Process Engineering, Department of Chemistry, Faculty of Sciences, Ibn Tofaïl University, B.P. 133, 14000 Kenitra, Morocco

resistant to conventional treatment methods, leading to their persistence in aquatic ecosystems and potential adverse effects on human health and the environment (El Hajam et al. 2019a; El Hassani et al. 2023; Solayman et al. 2023; Tanji et al. 2023a; El Messaoudi et al. 2024). Therefore, there is an urgent need to develop efficient and sustainable techniques to address the remediation of dye-contaminated wastewater.

One such synthetic dye of concern is Brilliant Green (BG), a cationic dye widely used in the textile, paper, and leather industries leading to water contamination and harmful health issues (El Hajam et al. 2019b; Nithya et al. 2020; Mahmood et al. 2022). However, these dyes have been reported to cause hypersensitivity, carcinogenicity, and toxicity to living organisms (Sood et al. 2015). BG poses significant health risks through skin contact, eye contact, ingestion, and inhalation. Prolonged or repeated exposure can damage target organs. Its decomposition releases harmful byproducts, including nitrogen oxides, carbon dioxide, and sulfur oxides. BG is known for its high stability and complex chemical structure, making it a challenging target for conventional treatment methods. This makes it an excellent candidate for studying the efficiency of photocatalysts. Various techniques have been employed to treat dye-containing effluents, but semiconductor photocatalysis has proven to be an effective and environmentally friendly technology (Kansal et al. 2013). Therefore, developing a practical and environmentally friendly approach to the degradation of BG dye is important.

Photocatalysis employs semiconducting materials to generate reactive oxygen species (ROS) under light irradiation, which can efficiently degrade organic compounds (Belghiti et al. 2022b; Tanji et al. 2023b). Among the various photocatalysts investigated, titanium dioxide (TiO_2) has gained considerable attention due to its high photosensitivity, stability, low cost, and non-toxicity (Nur et al. 2022). However, the efficient utilization of TiO_2 for dye degradation requires suitable modifications to overcome its limitations, such as restricted absorption capacity for non-polar organic contaminants, complications in photocatalyst recovery, the tendency of nano-sized catalysts to aggregate, and difficulties in achieving uniform catalyst distribution (El Gaidoumi et al. 2021; Balakrishnan et al. 2022; Suhan et al. 2023).

Based on the literature review, numerous studies have focused on the degradation of the BG molecule using various composites. One such study involves the use of gold nanoparticles with a polysaccharide nanocatalyst derived from Sesbania gum (SBG-AuNPs) as reported by Nagaraja et al. (Nagaraja et al. 2024). Another approach utilizes a reduced graphene oxide–zinc oxide nanocomposite (Yadav et al. 2024). Additionally, Prabagar et al. have explored the use of a nanofiber assembly of nickel iron aluminum layered double hydroxide (NiFeAl-LDH) combined with polyvinyl pyrrolidone (PVP) and polyvinyl alcohol (PVA), resulting in a fibrous matrix known as NiFeAl-LDH/PVP/PVA (Prabagar et al. 2024). Matussin et al. introduced Ni-doped $Gd(OH)_3$ nanorods as an effective material for BG molecule degradation (Matussin et al. 2024). Similarly, $Y_2Ti_2O_7$/AgO films have been investigated for their photocatalytic properties by Fernandez et al. (Fernandez et al. 2024) and Roy et al. developed a CuO-Ag_2O hybrid metal oxide composite using Carica papaya and hydroxyapatite derived from fish bone food waste (Roy et al. 2024). In another study, Mn-doped SnO_2 was employed by Ragupathy et al. for BG treatment (Ragupathy et al. 2023). Lastly, Rahman et al. studied the efficacy of $CdS@CuInS_2$ nanocomposites (Rahman et al. 2024). These various composites and nanomaterials demonstrate the extensive research efforts dedicated to developing effective solutions for the degradation of the BG molecule.

In recent years, the modification of photocatalysts by incorporating them into natural clay matrices has gained significant interest (El Gaidoumi et al. 2021, 2022). Natural clays offer several advantages such as abundant availability, low cost, high surface area, and adsorption capacity. The integration of TiO_2 with natural clay can enhance its stability and recyclability, and provide additional active sites for photocatalytic reactions (El-naggar et al. 2021; Zhan et al. 2021). Consequently, such composite materials hold great potential for efficiently degrading synthetic dyes.

In this context, these discoveries could offer additional contributions to the elaboration of new composites based on modified ZnO for various potential applications and especially photocatalysis. This study focuses on creating a new composite modified natural material /TiO_2 using wet impregnation method. It also aims to develop a straightforward technique for preparing such type of composites. The resulting composite was thoroughly characterized using various analytical instruments. Additionally, the study evaluates the composite's effectiveness in photocatalytically degrading BG dye from aqueous solutions, considering the impact of various operational parameters. Moreover, the study aims to optimize the process parameters to achieve maximum removal efficiency using the Box-Behnken design, a response surface methodology, to efficiently explore and determine optimal conditions, while minimizing the number of required experiments. This statistical approach enabled us to efficiently investigate the interactive effects of the chosen parameters and determine their optimal levels for achieving maximum BG dye removal efficiency. The choice of parameters was based on their known influence on photocatalytic degradation processes. The percentage of TiO_2 (%TiO_2) was selected to control the amount of photocatalyst in the composite, while the initial concentration of BG dye ([BG] ppm) and the pH of the

solution were crucial factors affecting the dye degradation kinetics. Finally, the wet impregnation synthesis method and dye removal using a non-toxic composite highlight the process's environmental friendliness.

Experimental materials and methods

Chemicals

All chemicals used in this study were purchased from Sigma-Aldrich including: Sodium hydroxide (NaOH, 98%), Phenol (C_6H_5OH, 99.5%), Titanium (IV) t-butoxide ($C_{16}H_{36}O_4Ti$, 97%), Formic acid (CH_2O_2, 98–100%), Oxalic acid ($C_2H_2O_4$, 99%), Maleic acid ($C_4H_4O_4$, 99%), Ascorbic acid ($C_6H_8O_6$, 99%), Hydrochloric acid (HCl, 37%), Acetonitrile (CH_3CN, 99.8%), Methanol (CH_3OH, 99.8%), Ethanol (C_2H_5OH, 99.5%), Hydrogen peroxide (H_2O_2, 30%), and Dimethyl sulfoxide ((CH_3)$_2$SO, 99%). Milli-Q water was used in all experiments.

Photocatalyst synthesis

The TiO_2 nanoparticles photocatalyst was synthesized using the sol–gel method described in previous work (Zouheir et al. 2022). After that, the initial step involved sourcing natural local material (NM), characterized by its brownish hue, from the northeastern region of Morocco. This material underwent an initial crushing and sieving process to achieve a finely homogeneous particle size of 60 μm. Subsequently, a mass of 0.9, 0.85, and 0.8 g of NM particles were integrated using the wet impregnation technique with 0.1, 0.15, and 0.2 g of TiO_2, resulting in the formation of NM + X% TiO_2 (X = 10, 15, and 20), respectively. These composite materials were dried at 100 °C for 12 h, then crushing and calcination at 500 °C for 2 h.

Materials characterization

To characterize the prepared catalysts, different techniques were used. Diffractometer X'PERT PRO (Cu Kα with λ = 1.5416 Å and radiation at 30 kV and 450 W) was used to study of X-ray diffraction patterns (XRD). Spectra analysis was performed by using HighScore Xpert plus software. The spectrometer VERTEX 70 using the KBr method operating at a resolution of 4 cm^{-1} and recorded in a range of 400–4000 cm^{-1} was the instrument used to perform the analysis of Fourier transform infrared spectra (FTIR). The samples' morphology was examined through Scanning Electron Microscopy (SEM) using a Jeol-IT500 HR microscope, with an acceleration voltage varying from 0.5 kV to 30 kV. UV–Visible diffuse reflectance spectra (DRS) were acquired employing a UV–Vis spectrophotometer (PerkinElmer Lambda 950) in the range 200–800 nm using

BaSO$_4$ as reference. Subsequently, bandgap values were deduced from Tauc plots by extrapolating the linear segment of a graph depicting $[F(R\infty)\cdot h\nu]^{1/2}$ against the energy of the exciting radiation.

Photocatalytic tests and BBD optimization

Photocatalytic degradation procedure

The photocatalytic experiments were carried out in a batch photoreactor with a UV lamp. A predetermined volume of BG solution was introduced into the photoreactor, and the desired amount of NM + TiO_2 catalyst was added to the solution under constant stirring. The suspension was allowed to equilibrate in the dark for 30 min to ensure adsorption–desorption equilibrium between the BG molecules and the catalyst surface. Subsequently, the UV light source was turned on, and the photodegradation process was initiated. UV photodegradation runs were performed in a batch reactor (100 mL) using an Osram Ultra-Vitalux lamp (nominal power of 300 W, and lamp current of 1.3 A) with a sunlike radiation spectrum as an illumination source. The intensity of the incident UVA light on the solution was measured with a PMA 2200 UVA photometer (Solar Light Co.) being ca. 130 W/m^2 (UVA PMA2110 sensor; spectral response 320–400 nm).

A stock solution of BG dye was prepared by dissolving a predetermined amount of BG dye in deionized water. Working solutions with different concentrations of BG were prepared by diluting the stock solution.

At the end of each photocatalytic test, a sample was collected and analyzed for BG dye degradation. The concentration of BG dye was monitored using UV–Visible spectrophotometry at the dye's characteristic absorption wavelength (625 nm). The degradation efficiency was calculated using the following equation:

$$BG\ degradation\ (\%) = \frac{C_i - C_t}{C_i} \times 100 \qquad (1)$$

Where C_i is the initial concentration of BG dye and C_t is the concentration of BG dye at time t.

Results and discussion

Materials characterization

The XRD pattern provides a detailed analysis of five samples, including natural material (NM), TiO_2, and three samples with varying levels of impregnated TiO_2 (at 10, 15, and 20%) on the NM (Fig. 1). The natural clay sample exhibits well-defined diffraction peaks corresponding to the crystalline reflections of $CaCO_3$ and SiO_2. Similar

Fig. 1 XRD of NM, TiO_2, and NM + X%TiO_2 (X = 10, 15, and 20)
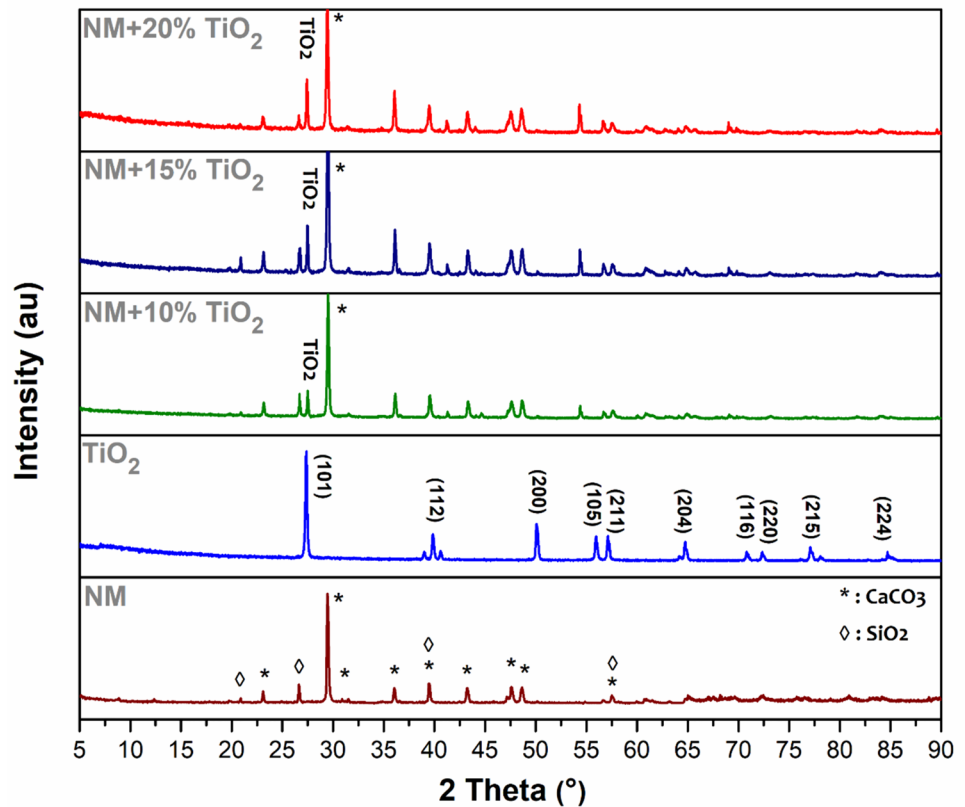
phases were found by Allali et al. at the same 2theta positions (Allali et al. 2014). However, the diffraction peaks observed at angles 27.41° (101), 39.84° (112), 49.19° (200), 55.79° (211), and 64.76° (204) confirm the synthesis of TiO_2 phase, which is in consistent with the JCPDS database (JCPDS #75–1537) (Zouheir et al. 2021). With the inclusion of 10% TiO_2 in the NM matrix, distinct TiO_2 peaks become increasingly prominent. As the TiO_2 concentration is further elevated, the intensity of these TiO_2 peaks experiences a proportional augmentation. The crystalline structure of the TiO_2 anatase is discernible, indicating its successful integration with the NM matrix (Zhang et al. 2009). This suggests a robust interaction between the two materials. This phenomenon underscores the progressive transformation of the crystallographic composition within the nanocomposite material. The introduction of TiO_2 initiates a series of structural changes, evidenced by the observed shifts in peak positions in the X-ray diffraction pattern. These shifts suggest potential lattice distortions induced by the presence of TiO_2 indicating its integration into the crystal lattice of the host material (Zhou et al. 2010). Such lattice distortions may lead to altered material properties, affecting mechanical strength, electronic behavior, and chemical reactivity (Hu et al. 2020.). Understanding these changes is crucial for optimizing the design and performance of TiO_2-based nanocomposites in various applications, ranging from catalysis to energy storage (Saqib et al. 2023).

The infrared spectra depicted in Figure 2 provide valuable insights into the chemical compositions and interactions of the analyzed samples. In the case of NM, distinctive absorption bands are evident. Notably, robust peaks around 1450 cm^{-1} and 800 cm^{-1} correspond to the bending and stretching vibrations of the carbonate ion within $CaCO_3$, while bands situated at 1050 cm^{-1} and 700 cm^{-1} imply Si-O stretching in SiO_2 (Stathatos et al. 2012), a conclusion supported by corroborative XRD analysis. The two vibrations intense bands at (1405 cm^{-1}, 871 cm^{-1}) which are elongation bands of C-O, and a less intense band appeared at 712 cm^{-1}, characteristics of the calcite. The shoulder at 1010 cm^{-1} (vibrations band of elongation Si-O) and the band at 469 cm^{-1} are assigned to quartz as already observed in XRD analysis. The TiO_2 spectrum exhibits characteristic features, including discernible bands approximately at 450 cm^{-1} attributed to Ti-O stretching vibrations and around 650 cm^{-1} correlating with Ti-O-Ti bending vibrations (Stathatos et al. 2012; Krishnan et al. 2017). The bond located at 800 cm^{-1} is related to metal oxide bonds such as titanium (Lin et al. 2017). With the augmentation of TiO_2 impregnation levels on the NM matrix, the prominence of TiO_2-associated peaks intensifies, reflecting the progressive inclusion of TiO_2. Simultaneously, alterations or shifts in peaks are pertinent to the interactions between TiO_2 and the matrix. This intriguing pattern is consistently observed across the spectra of samples impregnated with 10%, 15%, and 20% TiO_2, where

Fig. 2 FTIR spectra of NM, TiO$_2$, and NM + X%TiO$_2$ (X = 10, 15, and 20)
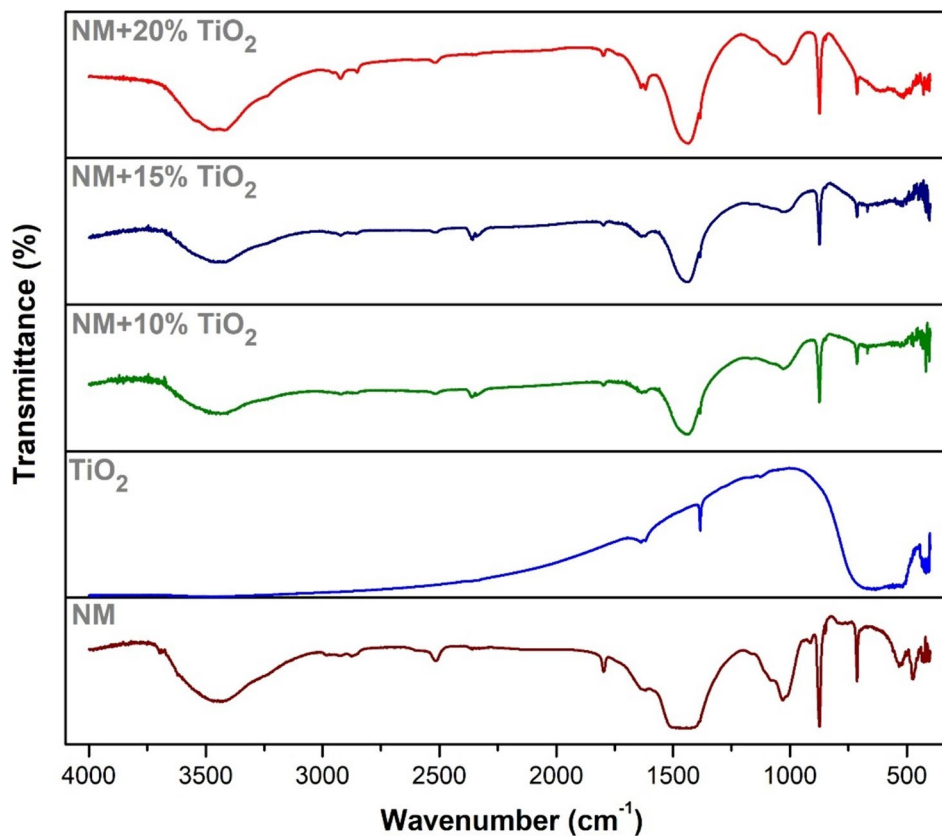
the reinforcement of TiO$_2$ signals and the evolving matrix characteristics collectively underscore the intricate interplay between these constituent elements. These comprehensive interpretations deepen our understanding of the spectral transformations, facilitating a more profound comprehension of the chemical dynamics resulting from impregnation and their implications for the ensuing material properties.

Figures 3 (a, b, c) illustrate the morphologies of the powders after TiO$_2$ impregnation. Upon closer examination, a comparison of the powders depicted in Figures 3 (a, b, c) underscores the presence of agglomerates in all three cases. Specifically, the powder containing 20%TiO$_2$ exhibits a finer granularity in contrast to the 15%TiO$_2$ counterpart, which, in turn, presents a finer structure compared to the 10% TiO$_2$ variant. Notably, the 10%TiO$_2$ powder displays a notably rough texture, coupled with more pronounced agglomeration. Across all three samples, homogeneity is generally noticed characterized by particles of both spherical and irregular morphology.

The EDX analysis, illustrated in Fig. 4, demonstrates a strikingly uniform elemental composition shared among all three samples. Calcium, silicon, oxygen, carbon, and titanium are consistently identified, affirming their fundamental presence in each sample's constitution. This convergence of elemental constituents strongly implies their integral role as building blocks within the material's composition.

Additionally, in the third sample, we observe the presence of aluminum, likely originating from the NM. These results confirm the successful wet impregnation of TiO$_2$ into the natural material with the desired percentage. This achievement underscores the effectiveness of the impregnation method in uniformly dispersing TiO$_2$ throughout the NM matrix.

The optical characteristics of the NM + X%TiO$_2$ composites were investigated through UV–vis spectroscopy and the absorption spectra are depicted in Fig. 5A. TiO$_2$ displays a broad absorption band in the UV range around 350 nm (Rossetto et al. 2010), whereas NM-TiO$_2$-(5,10 and 20%) exhibits more significant photon energy absorption around 350 nm which further confirms the successful combination of TiO$_2$ onto the NM (Li et al. 2018). In addition, NM + X%TiO$_2$ composites provide an enhanced absorption in the visible region compared to TiO$_2$ and NM alone due to the influence of the NM-TiO$_2$ combination (Li et al. 2018, 2022).

Tauc's plot was employed to estimate the bandgap energies (E$_g$) of NM-TiO$_2$- (5, 10, and 20%) using formula (2) (Mousavi et al. 2019).

$$(\alpha h v)^2 = A(h v - E_g) \tag{2}$$
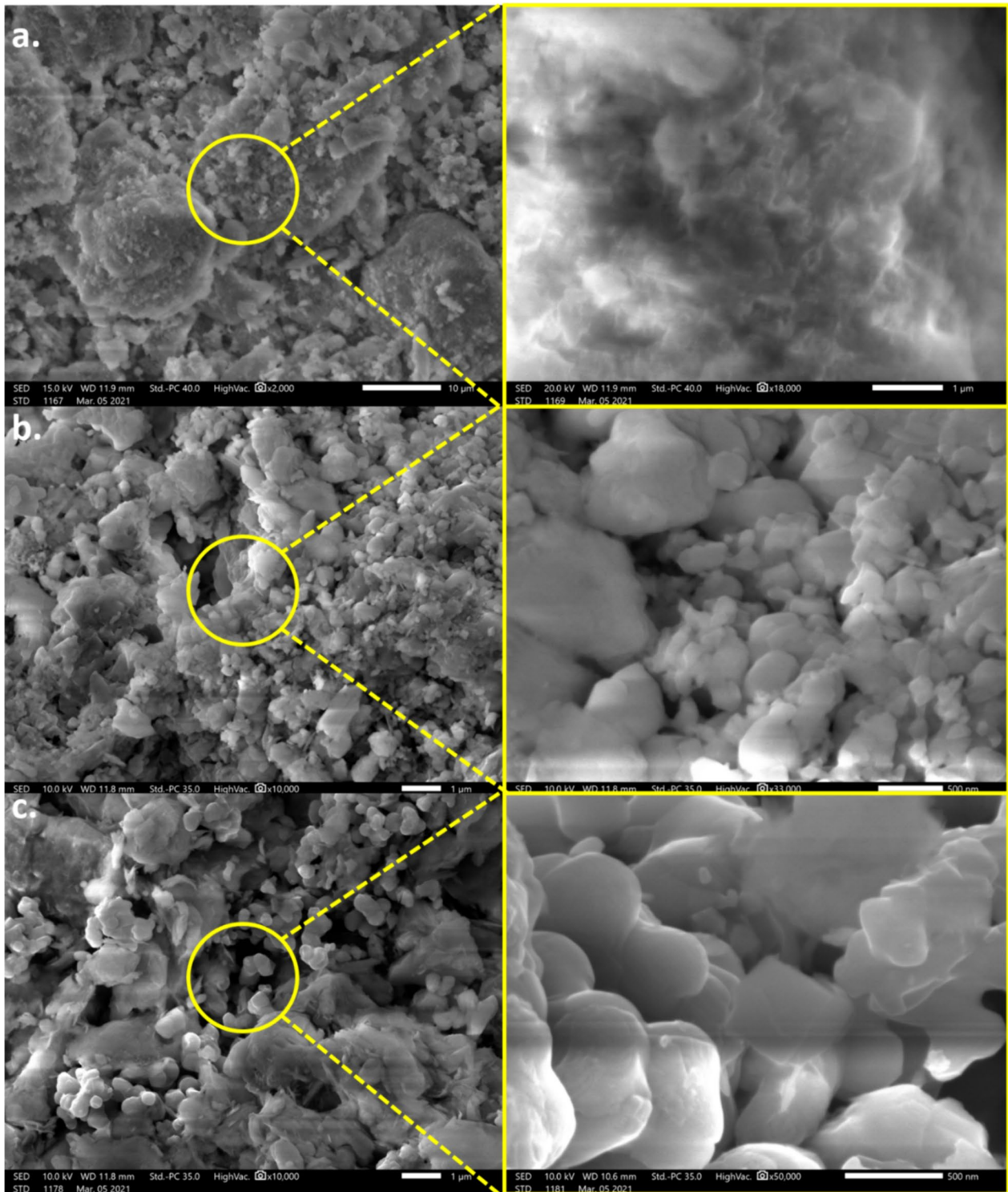
Fig. 3 SEM images of NM + X%TiO$_2$ **a** X = 10%, **b** 15%, and **c** 20%

Here, h, ν, α, and A represent Planck's constant, photon frequency, absorption coefficient, and a constant, respectively.

The optical band gaps were determined by extrapolating the linear region of $(\alpha h\nu)^2$ versus the photon energy axis (Fig. 5B). The calculated band gaps are 3.15 eV for TiO$_2$,
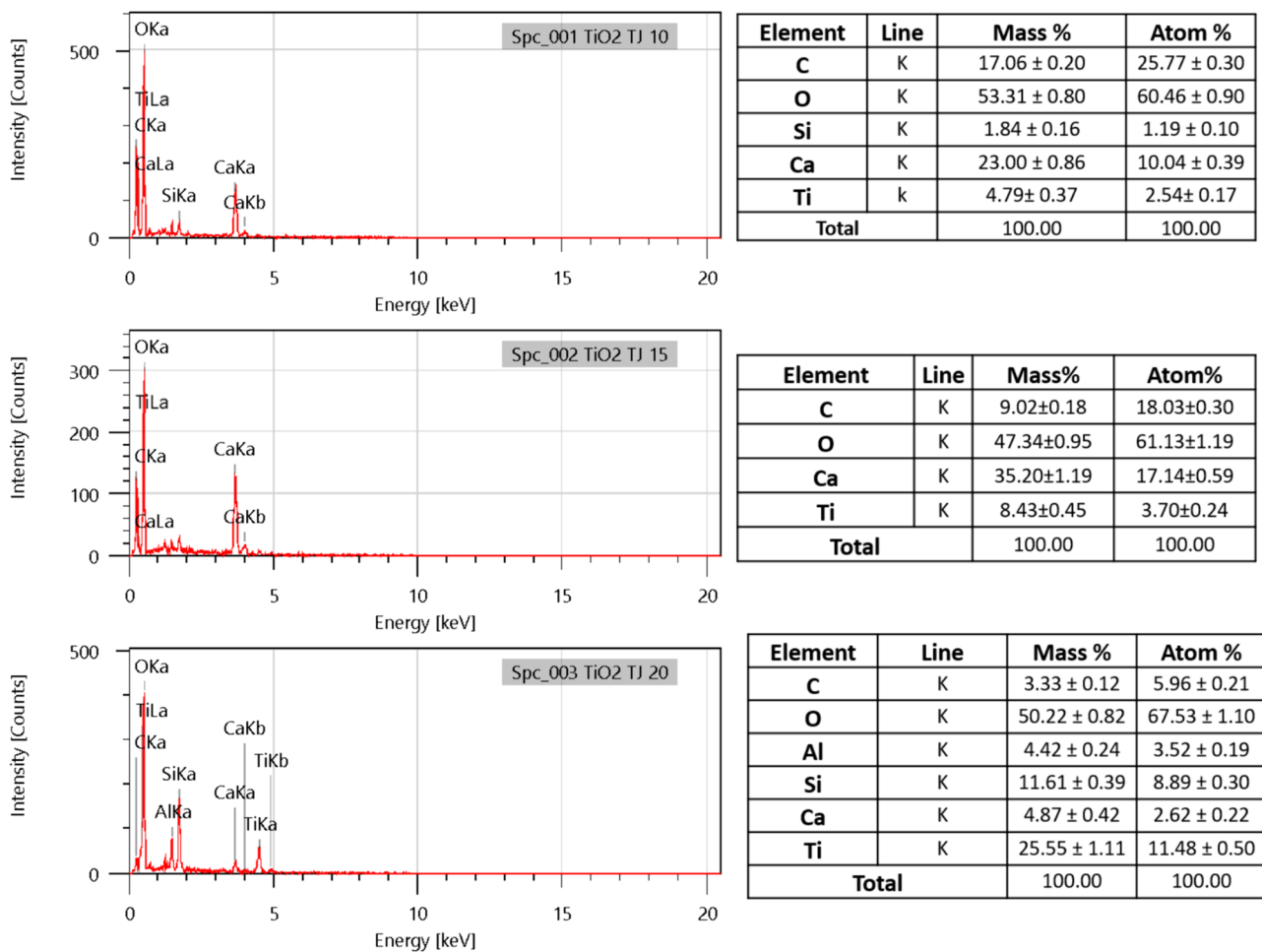
Element	Line	Mass %	Atom %
C	K	17.06 ± 0.20	25.77 ± 0.30
O	K	53.31 ± 0.80	60.46 ± 0.90
Si	K	1.84 ± 0.16	1.19 ± 0.10
Ca	K	23.00 ± 0.86	10.04 ± 0.39
Ti	k	4.79 ± 0.37	2.54 ± 0.17
Total		100.00	100.00

Element	Line	Mass%	Atom%
C	K	9.02±0.18	18.03±0.30
O	K	47.34±0.95	61.13±1.19
Ca	K	35.20±1.19	17.14±0.59
Ti	K	8.43±0.45	3.70±0.24
Total		100.00	100.00

Element	Line	Mass %	Atom %
C	K	3.33 ± 0.12	5.96 ± 0.21
O	K	50.22 ± 0.82	67.53 ± 1.10
Al	K	4.42 ± 0.24	3.52 ± 0.19
Si	K	11.61 ± 0.39	8.89 ± 0.30
Ca	K	4.87 ± 0.42	2.62 ± 0.22
Ti	K	25.55 ± 1.11	11.48 ± 0.50
Total		100.00	100.00

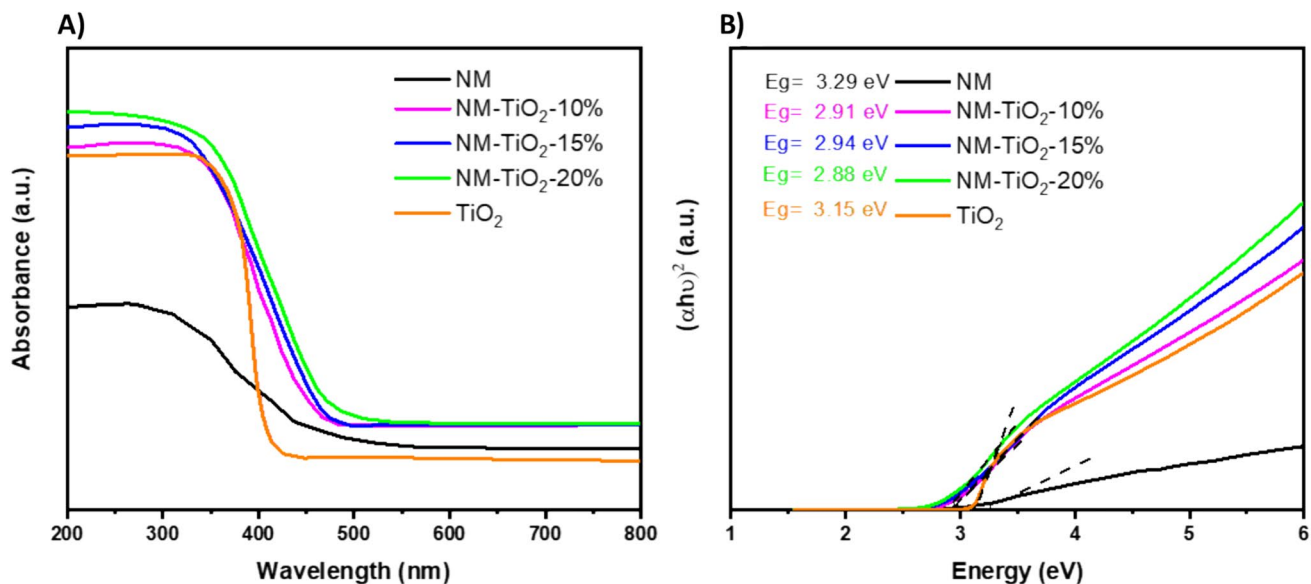**Fig. 4** EDX analysis of NM, TiO_2, and $NM + X\%TiO_2$ (X = 10, 15, and 20)

Fig. 5 (A) UV–vis DRS and (B) the plot of $(\alpha h\upsilon)^2$ versus energy ($h\upsilon$) of $NM + X\%TiO_2$ (X = 10, 15, and 20)

2.91 eV for NM-TiO$_2$-10%, 2.94 eV for NM-TiO$_2$-15%, 2.88 eV for NM-TiO$_2$-20%, respectively. Indeed, reducing the band gap is one of the most crucial parameters to enhance the efficiency of a photocatalyst system when using a source light with a lower wavelength.

Photocatalytic tests and BBD optimization

Table 1 displays the BBD matrix used to explore the effects of varying three factors on BG degradation (%), in a range of minimum (− 1) and maximum (+ 1) levels and a center point (0): TiO$_2$ content in the composite (%TiO$_2$ in %), pH in aqueous solution (pH), and BG concentration ([BG] in ppm).

Table 2 illustrates the analysis of variance (ANOVA). It helps identify the significance of individual factors and their interactions which aids in understanding which factors have the most influence on the response, enabling model refinement and informed decision-making. The coefficient of determination (R^2) and p-value are also fundamental metrics for evaluating the validity and significance of a statistical model. A higher R^2 signifies a better fit of the model to the observed data. On the other hand, the p-value assesses the significance of individual predictor variables and interactions within the model. A low *p*-value (typically below a predefined significance level of 0.05) suggests that the associated term is statistically significant, implying that it has a meaningful impact on the response variable. Moreover, a difference of less than 0.2 between the predicted R^2 and adjusted R^2 is required to confirm the model validity.

Hence, the results in Table 2 confirm the significance of the model with p-value < 0.0001, R^2 of ≈1, and reasonable

Table 1 Matrix of experiments and BG degradation percentage

Run	A:TiO$_2$ %	B:[BG] ppm	C:pH	BG degradation %
1	20	40	2	24
2	0	40	2	14
3	20	40	10	96
4	0	40	10	16
5	10	40	6	63
6	0	30	6	17
7	0	50	6	20
8	10	40	6	63
9	10	40	6	62
10	10	50	10	78
11	20	30	6	67
12	20	50	6	72
13	10	50	2	28
14	10	30	2	30
15	10	30	10	74

Table 2 ANOVA and fit statistics results

Source	Sum of Squares	Mean Square	F-value	p-value
Model	10,613.77	1179.31	80.59	< 0.0001
A-TiO$_2$	4608.00	4608.00	314.90	< 0.0001
B-[BG]	12.50	12.50	0.8542	0.3978
C-pH	3528.00	3528.00	241.09	< 0.0001
AB	1.00	1.00	0.0683	0.8042
AC	1225.00	1225.00	83.71	0.0003
BC	9.00	9.00	0.6150	0.4684
A^2	1046.26	1046.26	71.50	0.0004
B^2	12.41	12.41	0.8481	0.3993
C^2	256.41	256.41	17.52	0.0086

R^{2}0.9932

Adjusted R^{2}0.9808

Predicted R^{2}0.8913

agreement between the predicted R^2 and adjusted R^2. Moreover, the percentage of TiO$_2$ and pH are the most significant factors with positive effects, as their coefficients are positive in Eq. (3), on the model response. On the other hand, the BG concentration has no meaningful impact. It is plausible that at lower concentrations, active sites on the TiO$_2$ nanoparticles are efficiently utilized, leading to a saturation effect. Further increases in BG concentration may not result in a proportionate increase in degradation, as these sites are already occupied. Additionally, there might be an optimal concentration of BG for maximum photon absorption and utilization, beyond which additional molecules yield diminishing returns. Competing reactions or self-absorption by BG molecules at higher concentrations could also impede the photodegradation process (Groeneveld et al. 2023; Saqib et al. 2023).

After the model validation, the point with the highest BG removal under the optimal conditions was predicted. Table 3 outlines these results with predicted BG removal of 96.26% using 19.52% of TiO$_2$, BG concentration of 38.02 ppm, and pH of 9.91. To verify these findings an experimental test was carried out and the BG removal was well confirmed with 98.82%.

The final Eq. (3) which presents the response in terms of actual factors of the quadratic model was also exported.

Table 3 Prediction points of BG removal under the optimal conditions

Factor	Level	
TiO$_2$ (%)	19.52	Predicted BG removal: 96.26%
[BG] (ppm)	38.02	Experimental BG removal: 98.82%
pH	9.91	

$$\begin{aligned}
\text{BG degradation (\%)} = &-25.500 + 2.942\%\text{TiO}_2 + 1.317[\text{BG}] \\
&+ 5.625\,\text{pH} + 0.005\%\text{TiO}_2 * [\text{BG}] \\
&+ 0.438\%\text{TiO}_2 * \text{pH} + 0.038[\text{BG}] * \text{pH} \\
&-0.168\%\text{TiO}_2^2 - 0.018[\text{BG}]^2 - 0.521\,\text{pH}^2
\end{aligned}$$

$$(3)$$

In addition, the plot of the predicted vs. actual responses is considered a tool to assess the reliable prediction of the model. Figure 6 displays that almost all the points align perfectly along a diagonal line, it indicates that the model's predictions are almost exactly equal to the actual values.

Figure 7 depicts the two-dimensional (2D) contour plot that presents the BG removal as a function of the combination of two factors. Figure 7a indicates that by increasing the solution pH the BG degradation enhanced regardless of the BG concentration. This effect can be attributed to the higher proportion of OH^- ions in a basic environment, which promotes the formation of hydroxyl radicals through their reaction with positive holes (El Mouchtari et al. 2022). Similarly, by raising the $\%\text{TiO}_2$, the photodegradation efficiency of BG improved for all the values of its concentration (Fig. 7b). Which is due to the increase in TiO_2 particles on the surface of the NM. On the other hand, Fig. 7c exhibits the BG removal as a function of $\%\text{TiO}_2$ and solution pH, where the simultaneous increase of both factors led to the remarkable improvement of BG degradation.
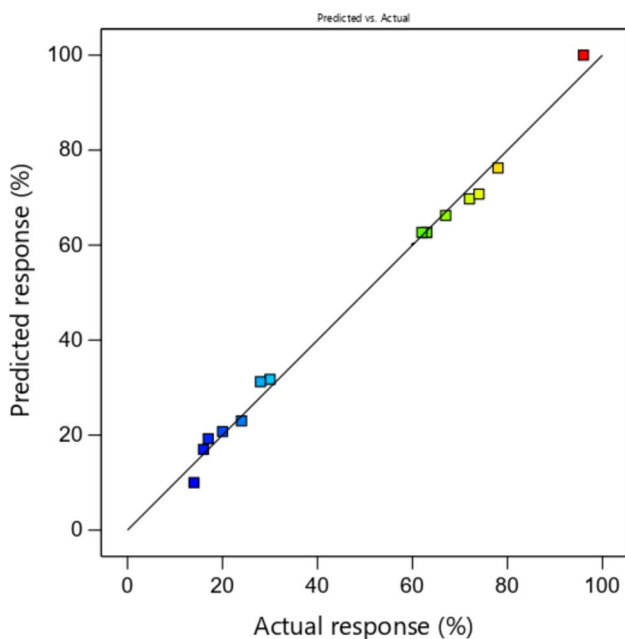

Fig. 6 Predicted as a function of actual response of BG removal

Comparison of adsorption and photocatalytic efficiency of the studied materials and scavenging and recyclability tests of NM + 20%TiO₂

The photocatalytic tests were carried out to investigate the photocatalytic efficiency of the prepared catalysts and raw NM. As shown in Fig. 8 TiO_2 alone can degrade 72% of BG molecule under UV illumination while NM alone does not exceed 33% which is the result of its adsorption including 25% during 30 min in the dark and 8% during 75 min under UV irradiation which confirm that the NM is not active under UV light. On the other hand, NM + 10%TiO₂ and NM + 15%TiO₂ show a photocatalytic efficiency of 90 and 94%, respectively, while NM + 20%TiO₂ presents the best efficiency and can degrade 98.82% of the BG dye. The combination of the adsorption proprieties of NM and the photocatalytic proprieties of TiO_2 could explain such a high BG removal.

To understand the degradation process of BG using NM + 20%TiO₂, the determination of radicals and holes responsible for the photocatalytic activity was done based on the results of scavenging tests. These experiments were based on the use of different scavengers: benzoquinone (BQ) for superoxide radical ($O_2^{\bullet-}$), silver nitrate (SN) for electrons (e^-), ethylene diamine tetra-acetic acid (EDTA-2Na) for (h^+) holes and isopropanol (IPA) for hydroxyl radical ($^{\bullet}OH$).

As presented in Fig. 9a, the degradation efficiency of BG decreased with the addition of isopropanol (IPA) and benzoquinone (BQ) compared to NS (No scavenger used). This can be related to the fact that the BG photodegradation is due to the reactive species superoxide radical ($O_2^{\bullet-}$) and the hydroxyl radical ($^{\bullet}OH$).

Figure 9b presents the results of the reusability tests of NM + 20%TiO₂ catalyst in the degradation of BG. These tests were based on the use of the same sample of catalyst in successive cycles with a simple wash with distilled water and drying in an oven. The obtained results indicate a good stability after five uses with a significant COD removal indicating a high mineralization.

Figure 10 presents linear regressions of $Ln(C/C_0)$ over time, confirming that the photodegradation of CV follows the Langmuir–Hinshelwood pseudo-first-order kinetics, as described by the equation $Ln(C/C_0) = kt$ (Shubha et al. 2022). This indicates that the rate of photodegradation is directly proportional to the concentration of BG at any given time. The photodegradation rate constants (k), which quantify the speed of the reaction, are found to be 0.011, 0.002, 0.021, 0.026 and 0.037 min^{-1} for TiO_2, NM, NM-TiO₂-10%, NM-TiO₂-15%, and NM-TiO₂-20% respectively. These values suggest that the addition of TiO_2 significantly enhances the photodegradation rate of BG, with the rate increasing as the TiO_2 content rises.
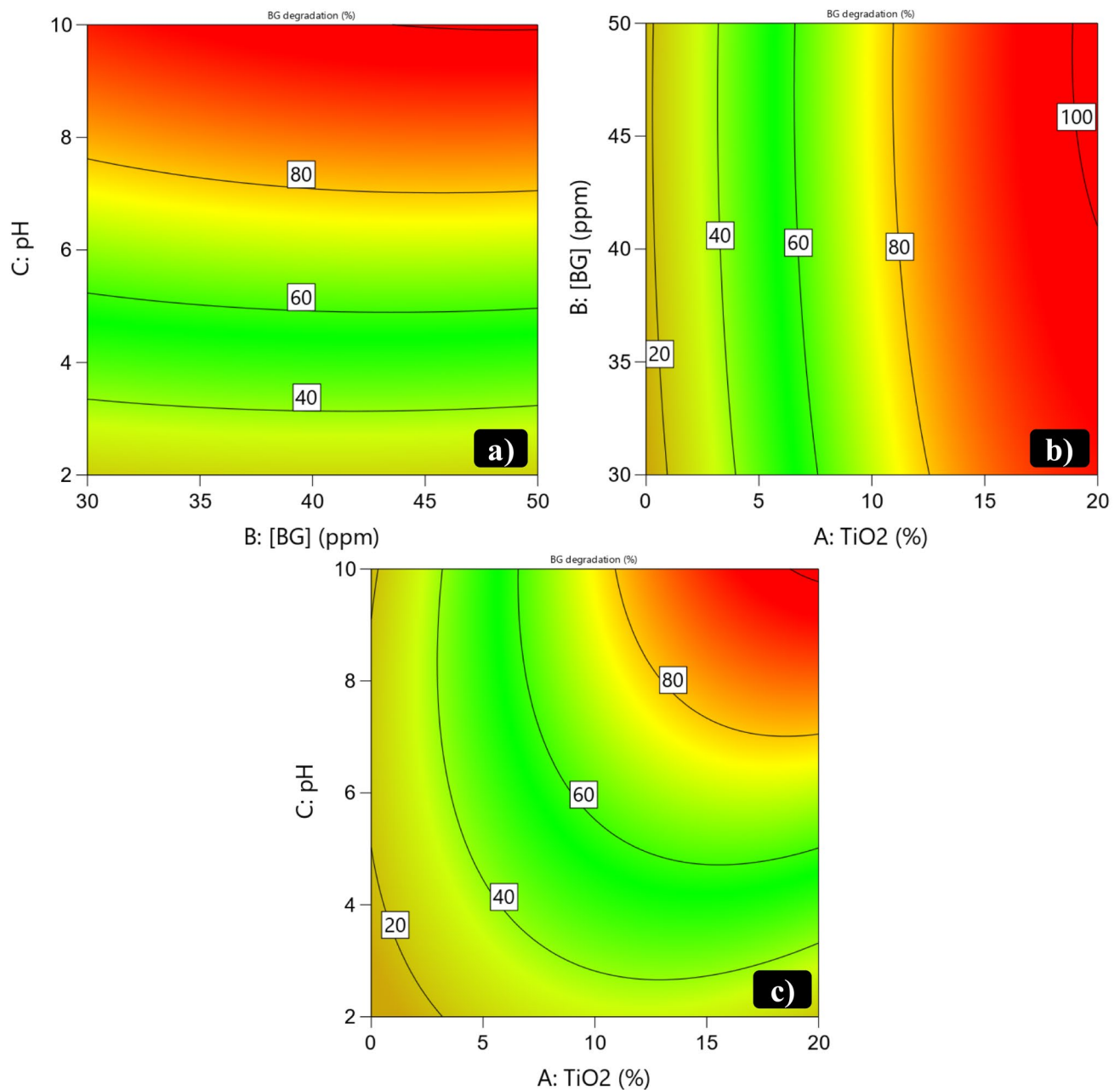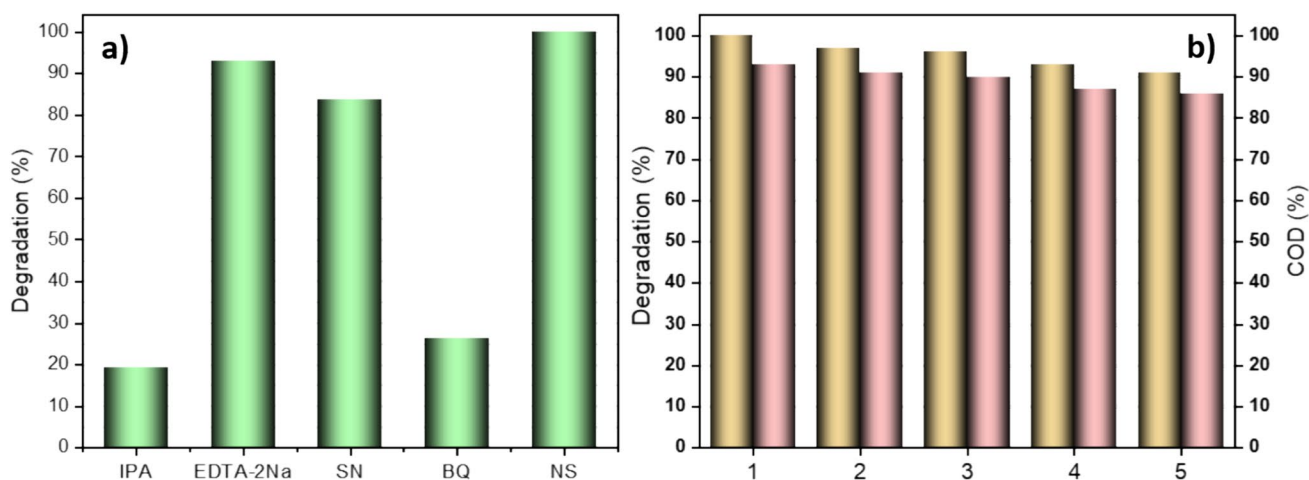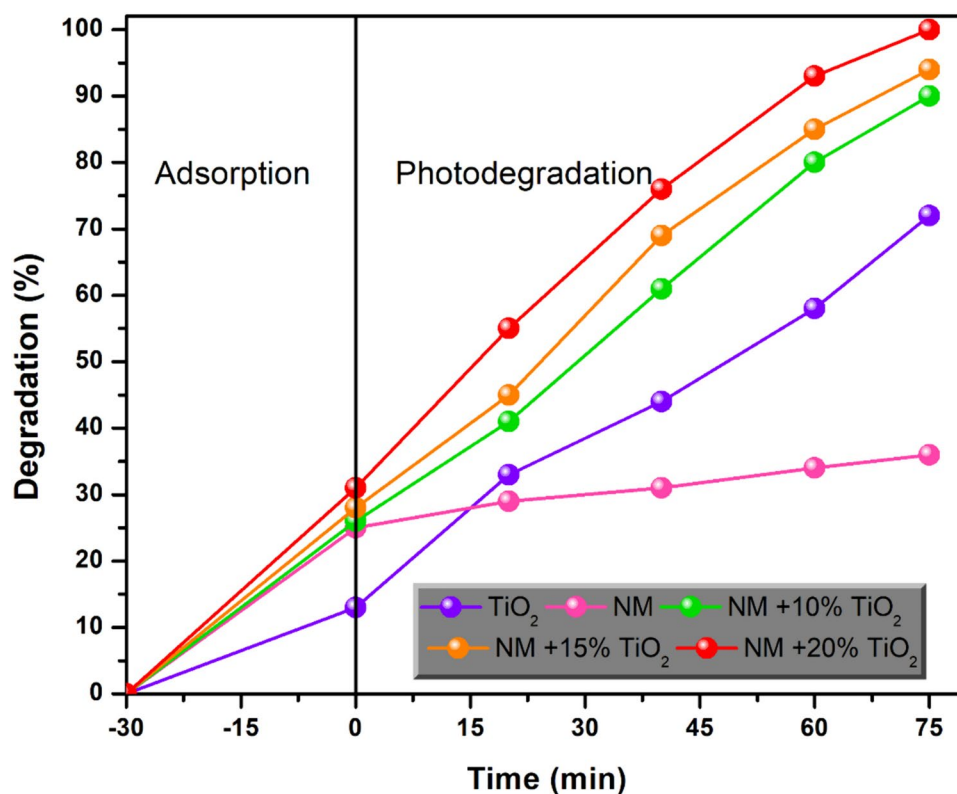
Fig. 7 Contour plots of BG removal against two factors: **a** pH and [BG] at %TiO$_2$ = 20%, b) [BG] and %TiO$_2$ at pH = 9.91 c) pH and %TiO$_2$ at [BG] = 38 ppm

Proposed mechanism

According to the above analysis, the photodegradation mechanism of BG (Fig. 11) involving the photocatalyst NM + 20%TiO$_2$ proceeds as follows: Firstly, the BG molecule was adsorbed on the NM + 20%TiO$_2$ surface. Thereafter, upon exposure to UV-light, TiO$_2$ within the composite catalyst absorbs photons, initiating the promotion of electrons from the valence band (VB) to the conduction band (CB), thereby generating electron–hole pairs

(e$^-$-h$^+$). Subsequently, electrons in the CB of TiO$_2$ react with adsorbed oxygen molecules (O$_2$) on the surface of NM to form superoxide radicals (O$_2$$^{\bullet-}$), while holes in the VB react with water molecules (H$_2$O) or hydroxide ions (OH$^-$) present in the environment to generate hydroxyl radicals ($^\bullet$OH) (Belghiti et al. 2022a). These superoxide and hydroxyl radicals, characterized by their high reactivity, act as potent oxidizing agents, initiating the attack and subsequent oxidation of the organic molecules comprising BG (Belghiti et al. 2022c). This leads to the fragmentation
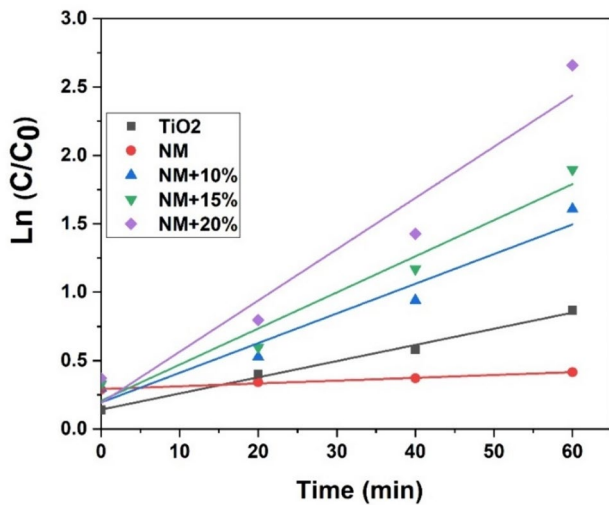
Fig. 8 BG removal over the studied materials under dark conditions (adsorption from -30 to 0 min) and UV irradiations (photocatalysis)

Fig. 9 **a** Active species trapping results and **b** Photocatalytic stability tests in terms of BG degradation and COD removal using NM + 20%TiO$_2$

of BG molecules, ultimately resulting in the breakdown of its complex chemical structure. The process continues until complete mineralization occurs, culminating in the conversion of organic contaminants into less harmful inorganic species. The final products of this photodegradation process typically consist of carbon dioxide (CO_2), water (H_2O), and inorganic ions, rendering them environmentally benign. This elucidates how the NM + 20%TiO$_2$ photocatalyst harnesses light energy to drive a cascade of
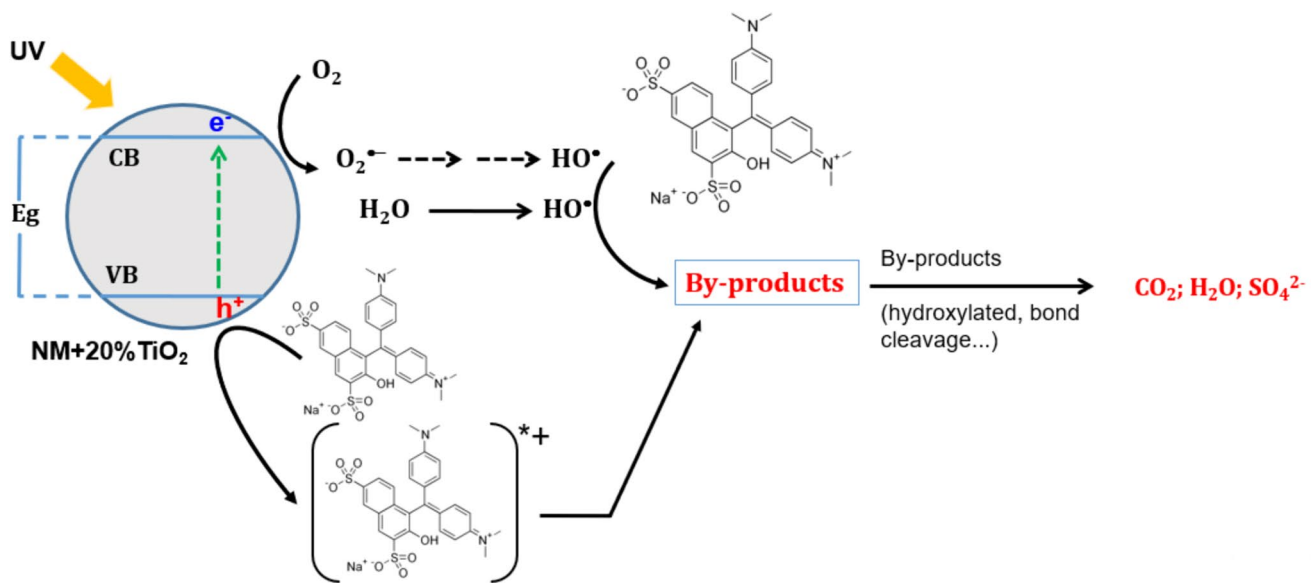
reactions that effectively degrade BG molecules, mitigating their environmental impact. Moreover, another degradation pathway suggests that photogenerated electrons (e^-) in the TiO$_2$ state can facilitate the reduction of adsorbed oxygen on the surface to produce superoxide radicals ($O_2^{\bullet-}$) during the electron transfer process. The transfer of photogenerated electrons to the NM framework occurs within femtoseconds. During this process, a continuous flow of electrons from the metal–semiconductor to the
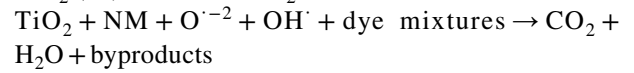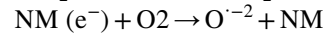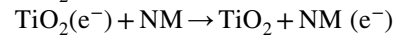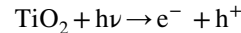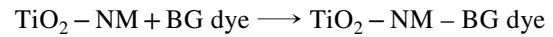
Fig. 10 ln (C/C_0) versus time plot of BG conversion using TiO_2, NM, NM-TiO_2-10%, NM-TiO_2-15%, and NM-TiO_2-20%

support material NM helps prevent recombination with holes by keeping the electrons away from TiO_2. The produced radicals are strongly oxidizing species that degrade CV molecules into simple inorganic molecules such as H_2O and CO_2, as found by Liu et al. (Liu et al. 2018). Furthermore, the valence band (VB) level of TiO_2 (3.15 eV vs. NHE) is higher than the standard redox potential of $^\bullet OH/OH^-$ (1.99 eV vs. NHE) (Ju et al. 2016). Consequently, the generated holes can oxidize H_2O or OH^- to produce $^\bullet OH$ radicals, which then degrade BG molecules. The proposed mechanism involves the following reactions:

Adsorption

$$TiO_2 - NM + BG\ dye \longrightarrow TiO_2 - NM - BG\ dye$$
$$TiO_2 + h\nu \rightarrow e^- + h^+$$
$$TiO_2(e^-) + NM \rightarrow TiO_2 + NM\ (e^-)$$
$$NM\ (e^-) + O2 \rightarrow O^{\cdot -2} + NM$$
$$TiO_2\ (h^+) + OH^- \rightarrow TiO_2 + OH^\cdot$$
$$TiO_2 + NM + O^{\cdot -2} + OH^\cdot + dye\ mixtures \rightarrow CO_2 + H_2O + byproducts$$

Comparison of BG photodegradation efficiency using NM + 20%TiO_2 and literature

Reviewing the literature reveals that BG photodegradation in aqueous solutions has been the subject of several investigations. Table 4 provides a comprehensive comparative analysis of the photodegradation performance under UV light utilizing various photocatalysts. Notably, the NM + 20% TiO_2 formulation showcases an impressive degradation rate of 98.82% for BG. This achievement is noteworthy when considering the relatively short removal time of 75 min and the modest concentration of the photocatalyst, which stands at just 100 ppm, especially in comparison to other photocatalysts referenced in the literature. It's important to acknowledge that the reported efficiencies in different studies may vary significantly due to many factors, such as diverse synthesis methods, variations in doping agents, differences in light sources, variations in solution pH, and initial concentrations of BG.

Fig. 11 proposed BG molecule degradation mechanism using NM + 20%TiO_2

Table 4 Comparison of various catalysts efficiency towards BG photodegradation

Photocatalyst	Photocatalyst concentration (ppm)	Irradiation Source	Time (min)	Degradation Efficiency (%)	References
Ag-CdO	80	Visible light	90	96	(Mahmood et al. 2022)
SnS	10,000	Sunlight	90	88	(Chowdhury et al. 2016)
$CoWO_4$ NPs	5000	Visible light	120	94	(Taneja et al. 2018)
CdSe-GO NPs	300	Sunlight	90	95	(Thirugnanam et al. 2017)
CeO_2/ZnO	2000	Visible light	50	91	(Jeyaraj et al. 2021)
TiO_2	2000	UV Light	120	99	(Munusamy et al. 2013)
$Fe_3O_4/CdS–ZnS$	100	Visible light	60	92	(Soltani-nezhad et al. 2020)
ZnO/CSAC	2000	Sunlight	120	90	(Nithya et al. 2020)
NM+20% TiO_2	100	UV light	75	98.82	This study

CSAC cotton stalk activated carbon (ZnO/CSAC), *NPs* Nanoparticles

Conclusion

In this paper, natural, abundant, and low-cost local material (NM)-based TiO_2-composite materials were successfully synthesized using an easy, environmentally friendly, and low-cost wet impregnation synthesis method. XRD, SEM, EDX, FTIR, and UV–vis results confirmed that TiO_2 was impregnated onto the natural local material (NM). BG degradation results using this new composite material, NM@TiO_2, under carefully optimized conditions revealed an impressive removal rate of up to 98.82%, demonstrating the potential of NM@TiO_2 as a highly efficient photocatalyst for environmental remediation applications. Optimization of key parameters such as the percentage of TiO_2 (20%), the initial BG concentration (38.02 ppm), and the pH level (9.91) was crucial to achieving this exceptional removal rate. The photocatalytic process benefited from the synergistic effects of NM and TiO_2, which enhanced adsorption capacity and photocatalytic activity, leading to significant degradation of BG molecules. The results of this study highlight the potential of NM@TiO_2 as a promising candidate for advanced wastewater treatment technologies, particularly for the removal of hazardous organic pollutants such as BG. However, further research is needed to explore the long-term stability and scale-up of this composite material under various environmental conditions, such as real effluents and industrial applications.

Data availability The data that support the findings of this study are available from the corresponding author upon reasonable request.

Declarations

Conflict of interest The authors declare that they have no conflict of interest.

Ethical approval This article does not involve any human participants and/or animals.

References

Allali F, Monsif M, Idrissi Kandri N, Zerouale A (2014) Caractérisation physico-chimique des enduits anciens et de restauration de la muraille (Al Moahades) bab chaâfa de la médina de salé: Etude comparative. J Mater Environ Sci 5:1577–1586

Balakrishnan A, Appunni S, Chinthala M (2022) Vo DVN (2022) Biopolymer-supported TiO_2 as a sustainable photocatalyst for wastewater treatment: a review. Environ Chem Lett 205(20):3071–3098. https://doi.org/10.1007/S10311-022-01443-8

Belghiti M, Mersly LEL, El MEM et al (2022a) Synthesis and characterization of Y2O3 partially coated ZnO for highly efficient photocatalytic degradation of sulfamethazine. J Mol Struct. https://doi.org/10.1016/j.molstruc.2021.132036

Belghiti M, Tanji K, El Mersly L et al (2022b) Fast and non-selective photodegradation of basic yellow 28, malachite green, tetracycline, and sulfamethazine using a nanosized ZnO synthesized from zinc ore. React Kinet Mech Catal 135:2265–2278. https://doi.org/10.1007/s11144-022-02232-8

Chowdhury AP, Shambharkar BH, Ghugal SG et al (2016) Ethylene glycol mediated synthesis of SnS quantum dots and their application towards degradation of eosin yellow and brilliant green dyes under solar irradiation. RSC Adv 6:108290–108297. https://doi.org/10.1039/C6RA10532G

El Gaidoumi A, Loqman A, Zouheir M et al (2021) Sol–gel fluorinated TiO_2–clay nanocomposite: study of fluor-titanium interaction on the photodegradation of phenol. Res Chem Intermed 47:1–26. https://doi.org/10.1007/s11164-021-04573-w

El Gaidoumi A, Tanji K, Loqman A et al (2022) Silver-photodeposited TiO_2-clay nanocomposite: sol–gel synthesis, characterization and CCD-optimized photocatalytic activity. J Iran Chem Soc 20:1–14. https://doi.org/10.1007/s13738-022-02668-8

El Hajam M, Idrissi Kandri N, Zerouale A (2019a) Batch adsorption of brilliant green dye on raw beech sawdust: equilibrium isotherms and kinetic studies. Moroccan J Chem. https://doi.org/10.48317/IMIST.PRSM/MORJCHEM-V7I3.16744

El Hajam M, Kandri NI, Harrach A, Zerouale A (2019b) Adsorptive removal of brilliant green dye from aqueous solutions using Cedar

and Mahogany Sawdusts. Sci Study Res Chem Chem Eng Biotechnol Food Ind 20:395–409

El Hassani AA, Tanji K, El Mrabet I et al (2023) A combined molecular dynamics simulation, DFT calculations, and experimental study of the adsorption of Rhodamine B dye on kaolinite and hydroxyapatite in aqueous solutions. Sur Interface 36:102647. https://doi.org/10.1016/J.SURFIN.2023.102647

El Messaoudi N, Franco DSP, Gubernat S et al (2024) Advances and future perspectives of water defluoridation by adsorption technology: a review. Environ Res 252:118857. https://doi.org/10.1016/J.ENVRES.2024.118857

El Mouchtari EM, Claeys-Bruno M, Rafqah S et al (2022) Optimisation of a photocatalytic water treatment using response surface methodology and quality by design Approach. Int J Environ Anal Chem. https://doi.org/10.1080/03067319.2021.2012171

El-naggar ME, Wassel AR, Shoueir K (2021) Visible-light driven photocatalytic effectiveness for solid-state synthesis of ZnO/natural clay/TiO_2 nanoarchitectures towards complete decolorization of methylene blue from aqueous solution. Environ Nanotech Monit Manag 15:100425. https://doi.org/10.1016/j.enmm.2020.100425

Fernandez L, Correa D, Seguel M et al (2024) Catalytic photo-degradation of brilliant green and bacterial disinfection of Escherichia coli by the action of Y2Ti2O7/AgO films. Ceram Int. https://doi.org/10.1016/J.CERAMINT.2024.04.255

Groeneveld I, Kanelli M, Ariese F, van Bommel MR (2023) Parameters that affect the photodegradation of dyes and pigments in solution and on substrate—an overview. Dye Pigment 210:110999. https://doi.org/10.1016/J.DYEPIG.2022.110999

Hu Y, Pan Y, Wang Z et al (2020) Lattice distortion induced internal electric field in TiO 2 photoelectrode for efficient charge separation and transfer. Nat Commun. https://doi.org/10.1038/s41467-020-15993-4

Jeyaraj M, Atchudan R, Pitchaimuthu S et al (2021) Photocatalytic degradation of persistent brilliant green dye in water using CeO2/ZnO nanospheres. Process Saf Environ Prot 156:457–464. https://doi.org/10.1016/J.PSEP.2021.10.033

Ju P, Wang Y, Sun Y, Zhang D (2016) Controllable one-pot synthesis of a nest-like Bi2WO6/BiVO4 composite with enhanced photocatalytic antifouling performance under visible light irradiation. Dalt Trans 45:4588–4602. https://doi.org/10.1039/C6DT00118A

Kansal SK, Lamba R, Mehta SK, Umar A (2013) Photocatalytic degradation of Alizarin Red S using simply synthesized ZnO nanoparticles. Mater Lett 106:385–389. https://doi.org/10.1016/J.MATLET.2013.05.074

Krishnan B, Mahalingam S, Bama K et al (2017) Ag / TiO_2 / bentonite nanocomposite for biological applications : synthesis, characterization, antibacterial and cytotoxic investigations. Adv Powder Technol 28:2265–2280. https://doi.org/10.1016/j.apt.2017.06.007

Li X, Peng K, Chen H, Wang Z (2018) TiO_2 nanoparticles assembled on kaolinites with different morphologies for efficient photocatalytic performance. Sci Rep 8:1–11. https://doi.org/10.1038/s41598-018-29563-8

Li H, Yao Y, Yang X et al (2022) Degradation of phenol by photocatalysis using TiO_2/montmorillonite composites under UV light. Environ Sci Pollut Res 29:68293–68305. https://doi.org/10.1007/s11356-022-20638-8

Lin L, Wang H, Xu P (2017) Immobilized TiO_2-reduced graphene oxide nanocomposites on optical fibers as high performance photocatalysts for degradation of pharmaceuticals. Chem Eng J 310:389–398. https://doi.org/10.1016/J.CEJ.2016.04.024

Liu Y, Yang Z-H, Song P-P et al (2018) Facile synthesis of Bi 2 MoO 6 /ZnSnO 3 heterojunction with enhanced visible light photocatalytic degradation of methylene blue. Appl Surf Sci 430:561–570. https://doi.org/10.1016/j.apsusc.2017.06.231

Mahmood K, Amara U, Siddique S et al (2022) Green synthesis of Ag@CdO nanocomposite and their application towards brilliant green dye degradation from wastewater. J Nanostructure Chem 12:329–341. https://doi.org/10.1007/S40097-021-00418-5

Matussin SN, Khan F, Harunsani MH et al (2024) (2024) Photocatalytic degradation of brilliant green and 4-nitrophenol using Ni-doped Gd(OH)3 nanorods. Sci Reports 141(14):1–11. https://doi.org/10.1038/s41598-024-58688-2

Mousavi S, Shahraki F, Aliabadi M et al (2019) Nanofiber immobilized CeO2/dendrimer nanoparticles: An efficient photocatalyst in the visible and the UV. Appl Surf Sci 479:608–618. https://doi.org/10.1016/j.apsusc.2019.02.119

Munusamy S, Aparna R, sai laxmi, Prasad R gunneswara subramanya vara, (2013) Photocatalytic effect of TiO_2 and the effect of dopants on degradation of brilliant green. Sustain Chem Process 1:1–8. https://doi.org/10.1186/2043-7129-1-4

Nagaraja K, Arunpandian M, Tae Hwan OH (2024) Enhanced photocatalytic degradation of organic pollutants by green-synthesized gold nanoparticles using polysaccharide for environmental remediation. Int J Biol Macromol 269:131866. https://doi.org/10.1016/J.IJBIOMAC.2024.131866

Nithya R, Ragupathy S, Sakthi D et al (2020) Photocatalytic efficiency of brilliant green dye on ZnO loaded on cotton stalk activated carbon. Mater Res Express 7:075002. https://doi.org/10.1088/2053-1591/ABA025

Nur ASM, Sultana M, Mondal A et al (2022) A review on the development of elemental and codoped TiO_2 photocatalysts for enhanced dye degradation under UV–vis irradiation. J Water Process Eng 47:102728. https://doi.org/10.1016/J.JWPE.2022.102728

Prabagar JS, Tenzin T, Sneha Y et al (2024) Novel NiFeAl hybridized layered double hydroxide nanofibrous for photocatalytic degradation and CO2 reduction. Mater Today Sustain 26:100773. https://doi.org/10.1016/J.MTSUST.2024.100773

Ragupathy S, Ramasundaram S, Thennarasu G et al (2023) Effect of Mn doping on structural, optical and photocatalytic properties of SnO2 nanoparticles. Ceram Int 49:17776–17783. https://doi.org/10.1016/J.CERAMINT.2023.02.143

Rahman A, Khan F, Jennings JR et al (2024) CdS@CuInS2 nanocomposites for enhanced photocatalytic activity under visible light irradiation. Mater Sci Semicond Process 177:108365. https://doi.org/10.1016/J.MSSP.2024.108365

Rossetto E, Petkowicz DI, dos Santos JHZ et al (2010) Bentonites impregnated with TiO_2 for photodegradation of methylene blue. Appl Clay Sci 48:602–606. https://doi.org/10.1016/j.clay.2010.03.010

Roy SD, Das KC, Dhar SS (2024) Facile synthesis of CuO-Ag2O hybrid metal oxide composite using carica papaya, cocooning with hydroxyapatite, and photocatalytic degradation of organic dyes. Mater Sci Eng B 303:117331. https://doi.org/10.1016/J.MSEB.2024.117331

Saqib M, Rahman N, Safeen K et al (2023) Structure phase-induced photodegradation properties of cobalt-sulfur co-doped TiO_2 nanoparticles synthesized by hydrothermal route. J Mater Res Technol 26:8048–8060. https://doi.org/10.1016/J.JMRT.2023.09.151

Shubha JP, Kavalli K, Adil SF et (2022) Facile green synthesis of semiconductive ZnO nanoparticles for photocatalytic degradation of dyes from the textile industry: a kinetic approach. J King Saud Univ - Sci 34:102047. https://doi.org/10.1016/J.JKSUS.2022.102047

Solayman HM, Hossen MA, Abd Aziz A et al (2023) Performance evaluation of dye wastewater treatment technologies: a review. J Environ Chem Eng 11:109610. https://doi.org/10.1016/J.JECE.2023.109610

Soltani-nezhad F, Saljooqi A, Mostafavi A, Shamspur T (2020) Synthesis of Fe3O4/CdS–ZnS nanostructure and its application for photocatalytic degradation of chlorpyrifos pesticide and brilliant

green dye from aqueous solutions. Ecotoxicol Environ Saf 189:109886. https://doi.org/10.1016/J.ECOENV.2019.109886

Sood S, Umar A, Kumar Mehta S et al (2015) Efficient photocatalytic degradation of brilliant green using Sr-doped TiO$_2$ nanoparticles. Ceram Int 41:3533–3540. https://doi.org/10.1016/J.CERAMINT.2014.11.010

Stathatos E, Papoulis D, Aggelopoulos CA et al (2012) TiO$_2$/palygorskite composite nanocrystalline films prepared by surfactant templating route: Synergistic effect to the photocatalytic degradation of an azo-dye in water. J Hazard Mater 211–212:68–76. https://doi.org/10.1016/j.jhazmat.2011.11.055

Suhan MBK, Al-Mamun MR, Farzana N et al (2023) Sustainable pollutant removal and wastewater remediation using TiO$_2$-based nanocomposites: a critical review. Nano-Structures & Nano-Objects 36:101050. https://doi.org/10.1016/J.NANOSO.2023.101050

Taneja P, Sharma S, Umar A et al (2018) Visible-light driven photocatalytic degradation of brilliant green dye based on cobalt tungstate (CoWO4) nanoparticles. Mater Chem Phys 211:335–342. https://doi.org/10.1016/J.MATCHEMPHYS.2018.02.041

Tanji K, El Mrabet I, Fahoul Y et al (2023a) Epigrammatic progress on the photocatalytic properties of ZnO and TiO$_2$ based hydroxyapatite@photocatlyst toward organic molecules photodegradation: A review. J Water Process Eng 53:103682. https://doi.org/10.1016/J.JWPE.2023.103682

Tanji K, El Mrabet I, Fahoul Y et al (2023b) Experimental and theoretical investigation of enhancing the photocatalytic activity of Mg doped ZnO for nitrophenol degradation. React Kinet Mech Catal 136:1125–1142. https://doi.org/10.1007/s11144-023-02385-0

Thirugnanam N, Song H, Wu Y (2017) Photocatalytic degradation of brilliant green dye using CdSe quantum dots hybridized with graphene oxide under sunlight irradiation. Chinese J Catal 38:2150–2159. https://doi.org/10.1016/S1872-2067(17)62964-4

Yadav P, Kapil I, Dutta M, Bhaduri A (2024) Effectual visible-driven photocatalytic performances on brilliant green dye by reduced graphene oxide–zinc oxide nanocomposite. Ionics (kiel) 30:2927–2937. https://doi.org/10.1007/S11581-024-05450-3/METRICS

Zhan J, Chen H, Zhou H et al (2021) Mt-supported ZnO/TiO$_2$ nanocomposite for agricultural antibacterial agent involving enhanced antibacterial activity and increased wettability. Appl Clay Sci 214:106296. https://doi.org/10.1016/j.clay.2021.106296

Zhang W, Zou L, Wang L (2009) Photocatalytic TiO$_2$/adsorbent nanocomposites prepared via wet chemical impregnation for wastewater treatment: a review. Appl Catal A Gen 371:1–9. https://doi.org/10.1016/J.APCATA.2009.09.038

Zhou W, Liu Q, Zhu Z, Zhang J (2010) Preparation and properties of vanadium-doped TiO$_2$ photocatalysts. J Phys D Appl Phys 43:035301. https://doi.org/10.1088/0022-3727/43/3/035301

Zouheir M, Assila O, Tanji K et al (2021) Bandgap optimization of sol–gel-derived TiO$_2$ and its effect on the photodegradation of formic acid. Nano Futur 5:25–29. https://doi.org/10.1088/2399-1984/abfb7d

Zouheir M, Tanji K, Navio JA et al (2022) Effective photocatalytic conversion of formic acid using iron, copper and sulphate doped TiO$_2$. J Cent South Univ 29:3592–3607. https://doi.org/10.1007/s11771-022-5172-9